A General and Effective Mode Filtering Method for the Suppression of Clutter in Far-Field Antenna Measurements

S.F. Gregson[1, 2], C.G. Parini[1], A.C. Newell[3]

[1]Queen Mary University of London
School of Electronic Engineering and Computer Sciences
Peter Landin Building,
10 Godward Square
London UK E1 4FZ

[2]National Physical Laboratory
Hampton Road, Teddington, UK, TW11 0LW

[3]Newell Near-Field Consultants,
2305 Vassar Drive,
Boulder, CO 80305

stuart.gregson@qmul.ac.uk, c.g.parini@qmul.ac.uk, allen_newell@qwestoffice.net

***Abstract*—The use of mode filtering to improve the quality of antenna measurements taken in non-anechoic environments is well known, [1, 2, 3, 4, 5]. In the far-field case [6, 7, 8], it has been shown that it is possible to use standard cylindrical near-field theory [8] to implement the necessary mode filtering using a singularly polarized, great circle, far-field pattern cut consisting of amplitude and phase data. The careful verification of this technique using a compact antenna test range (CATR) was reported in [7, 8] however that implementation had, as a prerequisite, the need to acquire the far-field data on a monotonic and equally spaced pattern abscissa. In many instances this is not convenient or perhaps impossible. This paper presents a recent development which allows data to be processed rigorously when having been acquired using an unequally spaced angular abscissa. This paper sets out the novel, far more sophisticated, algorithm together with results of actual range measurements that were processed using this new technique.**

I. INTRODUCTION

A far-field antenna pattern is characterised by exhibiting a spatial variation that has an angular dependence, *i.e.* an: angular amplitude variation, angular phase variation and angular polarisation variation. Ideally, all of these properties can be measured by placing the antenna under test (AUT) in a perfectly uniform, homogeneous, plane wave field and by mechanically rotating it while measuring the received amplitude and/or phase [8]. In practice, perhaps the most straightforward measurement method is to approximate a plane wave front, locally, over the AUT from a small portion of a spherical wave-front with a large radius. This can be achieved by placing a low gain source antenna at a large physical and electrical distance from the AUT so that the field illuminating the antenna's aperture very closely approximates a transverse electric and magnetic (TEM) plane-wave. An alternative way to produce a TEM wave is to use the very carefully controlled reflection from a precisely curved conducting surface to collimate the field radiated by the source antenna into a plane–wave. The popularity of these compact antenna test ranges (CATR), *i.e.* compact when compared to a point-source far-field range, can perhaps be seen to stem from the simplicity with which far-field parameters can be obtained from the experimental equipment, the absence of a requirement to undertake intensive mathematical post-processing before useful results can be obtained, and the ability to very efficiently acquire zero-dimensional (*e.g.* boresight) and one-dimensional (*e.g.* great circle cut) data.

Reflections in antenna measurement systems can often be seen to comprise the single largest component of measurement uncertainty within the uncertainty budget of a given range [8]. Considerable space has been devoted to the subject of range multipath suppression in the open literature with a great deal of time, effort, and ingenuity being directed towards quantifying and subsequently extracting reflected fields from antenna pattern measurements [1, 2, 3, 4, 5, 6, 7, 8]. The mode orthogonalisation and filtering techniques that have proved so overwhelmingly successful in near-field applications (planar, cylindrical, spherical) were only comparatively recently extended for use with far-field ranges [6, 7] for improving one [6, 7] and two-dimensional [8] antenna pattern data. However, although these techniques have proved to be very successful in processing far-field data,

they have been predicated upon the availability of data sampled on a monotonic and equally spaced abscissa. While this is something that can, to a large extent, be assumed to be available when taking near-field measurements, the same is not necessarily true for the far-field case. The following section presents the development of a new, general purpose, correction technique with the subsequent section then illustrating the success of this technique with actual range measurements.

II. Generalised Approach to Far-Field Mode Filtering

In general, when we take near-field measurements we do so by acquiring data across a convenient surface which bounds the radiator. We have a forward transmission equation which we invert to solve for the unknown mode coefficients of the vector basis functions that are commensurate with the surface that we are testing on. Once we know this set of mode coefficients, we can correct them for the directive and polarisation properties of the measuring probe. We then use these compensated mode coefficients with the forward transmission equation to solve for the field anywhere outside of the near-field sampling surface including the far-field region where, asymptotically, we choose a spherical surface of infinite radius. So that we may develop the generalised post-processing let us start by taking the standard transmission equation [8] which relates cylindrical mode coefficients (CMC) to far-fields where, as per the usual convention, the unimportant far-field spherical phase factor and inverse r term have been suppressed,

$$E_\theta(\theta,\phi) = 2jk_0 \sin\theta \sum_{n=-\infty}^{\infty} (-j)^n B_n^2(\gamma) e^{jn\phi} \tag{1}$$

Here, for a fixed measurement radius and frequency the electric field can be expressed in terms of mode coefficients, which are complex numbers that do not vary with any of the measuring coordinates and are instead functions of n, the angular index and γ the Fourier variable. Thus, for the case where $\theta = \pi/2$ radians, *i.e.* the case of a great circle far-field pattern cut, the electric field can be expressed as,

$$E_\theta(\phi) = 2jk_0 \sum_{n=-\infty}^{\infty} (-j)^n B_n^2 e^{jn\phi} \tag{2}$$

With no loss of generality, we may rewrite this summation in the form of a matrix multiplication yielding,

$$\begin{bmatrix} E_{\theta,\phi_1} \\ E_{\theta,\phi_2} \\ \vdots \\ E_{\theta,\phi_{n_\phi}} \end{bmatrix} = 2jk_0 [M] \cdot \begin{bmatrix} B_1^2 \\ B_2^2 \\ \vdots \\ B_n^2 \end{bmatrix} \tag{3}$$

Here, the matrix of basis functions M which has n_ϕ rows by n_n columns is defined as,

$$[M] = \begin{bmatrix} -je^{j\phi_1} & (-j)^2 e^{j2\phi_1} & \cdots & (-j)^{n_n} e^{jn_n\phi_1} \\ -je^{j\phi_2} & (-j)^2 e^{j2\phi_2} & \cdots & (-j)^{n_n} e^{jn_n\phi_2} \\ \vdots & \vdots & \ddots & \vdots \\ -je^{j\phi_{n_\phi}} & (-j)^2 e^{j2\phi_{n_\phi}} & \cdots & (-j)^{n_n} e^{jn_n\phi_{n_\phi}} \end{bmatrix} \tag{4}$$

Here, the elements within the matrix M have a magnitude of unity with only the phase varying from element to element. Inverting this expression and simplifying yields,

$$\begin{bmatrix} B_1^2 \\ B_2^2 \\ \vdots \\ B_n^2 \end{bmatrix} = -\frac{j}{2k_0} [M]^{-1} \cdot \begin{bmatrix} E_{\theta,\phi_1} \\ E_{\theta,\phi_2} \\ \vdots \\ E_{\theta,\phi_{n_\phi}} \end{bmatrix} \tag{5}$$

This matrix equation expresses the unknown CMCs in terms of the far-field points. A similar expression can be obtained for the orthogonal field component and second independent set of CMCs. In inverting this system of equations we have assumed that the matrix M is a non-singular square matrix and the superscript -1 denotes the matrix inverse such that by definition $M^{-1}M = I$ where I is the identity matrix. In general the matrix M will *not* be square and we will need to find its inverse using some degree of estimation. Fortunately, we can find a pseudo inverse matrix by using the principle of least squares to obtain an approximate solution. From equation (3) and multiplying by the Hermitian (conjugate) transpose of M we obtain,

$$M^T M b = M^T v \tag{6}$$

Here v, is a column vector set of measurements, M is a matrix of basis functions, *i.e.* wave functions, and b is a column vector set of unknown mode coefficients and M^T is the Hermitian transpose of M. Thus when the columns of M are linearly independent, the product $M^T M$ is invertible and we may write that,

$$b = \left(M^T M\right)^{-1} M^T v = M^P v \tag{7}$$

Where, M^p denotes the pseudo inverse matrix. Thus, we can obtain the set of unknown mode coefficients from the set of measurements and the pseudo inverse matrix of basis functions using,

$$\begin{bmatrix} B_1^2 \\ B_2^2 \\ \vdots \\ B_n^2 \end{bmatrix} = -\frac{j}{2k_0} M^P \cdot \begin{bmatrix} E_{\theta,\phi_1} \\ E_{\theta,\phi_2} \\ \vdots \\ E_{\theta,\phi_{n_\phi}} \end{bmatrix} \tag{8}$$

Although this looks to be a reasonable strategy, the difficulty associated with this approach is that the matrix M will, for any practical measurement, be fairly large. However, as the far-field measured data comprises a pattern cut, this matrix will likely be much smaller than would otherwise be the case if two-dimensional pattern data were under consideration. Hence, alternative more efficient methods for computing the pseudo inverse are generally needed with the iterative conjugate gradient (CG) method [10] or least squares conjugate gradient (LSQR) method [11] being popular choices. The LSQR method is a particular implementation of the CG method which offers a numerically stable and computationally efficient solution for the inversion of the matrix M. A detailed treatment of the LSQR is beyond the scope of this paper and is instead left to the open literature *cf.* [11].

When constructing the matrix of basis functions consideration must be taken as to the number and range of CMCs that are needed. The highest order cylindrical mode that can be computed from the far-field measured data can be determined from the arithmetic mean sample spacing using [8],

$$n_{\mathrm{Max}} = \mathrm{ceil}\left(\frac{\pi}{|\Delta\phi|}\right) \tag{9}$$

Here, ***ceil*** is used to denote a function that rounds to the nearest integer towards positive infinity. In this case, $\Delta\phi$ is taken to be the arithmetic mean angular sample spacing between the data points. Providing that the data points are not *too* unevenly distributed, this formula will provide a reliable estimate of the highest order mode that can be reliably computed. Thus, the range of modes will span $-n_{\mathrm{Max}} \le n \le n_{\mathrm{Max}}$. As this algorithm does not utilise the FFT there is no need to have the number of modes equal an integer power of two. Thus, we are free to choose the number of modes, N, as being,

$$N = 2n_{\mathrm{Max}} + 1 \tag{10}$$

The computed modes can be filtered using a band-pass windowing function so that only those modes which are associated with the AUT are retained [6, 7, 8] whereupon the filtered far-fields can be obtained from an application of equation (3). Although we can, for the sake of computational efficiency, use the pre-computed M matrix so that the filtered fields are reconstructed at the measurement points, we are of course free to choose a different M matrix so that the reconstructed far-field points can be tabulated on an, *e.g.* equally spaced, grid of our choosing.

III. Preliminary Results

The Queen Mary University of London (QMUL) mm-wave Compact Antenna Test Range (CATR) is formed from a single sector shaped offset reflector antenna with a 3 metre diameter reflector and is constructed from 18 individual high precision panels where the individual panels have a measured average root mean squared (RMS) surface accuracy of between 8 and 15 microns. Each panel has three, micrometer adjustable, mounting points which are individually optically aligned providing an overall surface RMS accuracy of approximately 90μm. An anechoic chamber completely encloses the mm-wave CATR to control and minimise the range reflections. The QMUL CATR is described in detail in reference [9] and is presented in Figure 1.

In the absence of some overriding definitive standard or infallible (truth) model, the only practical methodology for examining the effectiveness of a new processing technique is by way of measurement repetition. This repetition can be accomplished without alteration to the measurement configuration, to simply address repeatability, or with the inclusion of some parametric change whereupon it can be used to assess sensitivity to that particular change. In this case, repeat measurements were taken of the far-field great circle azimuth cut of a medium gain (aperture diameter 127mm) x-band corrugated horn where a single parametric change was introduced into the measurement. This change comprised the introduction of a 0.6 m by 0.6 m flat reflecting plate that was located in the same horizontal plane as the AUT. This was chosen to constitute a worst case scattering configuration as the specular reflection of the main beam of the corrugated horn directly illuminated the CATR reflector. This configuration can be seen presented in Figure 1. This system was used to acquire far-field amplitude and phase pattern data as a function of angle. However, the measurements were taken at regular intervals in time since this process was known to be the most accurate technique for recording data within this facility. Although the data was sampled using a regular time basis, the acceleration of the positioner resulted in the data being tabulated on an irregularly spaced angular grid. However, at a typical rate of 15 samples per decimal degree, this data was grossly over sampled when compared to the angular increment suggested by the cylindrical sampling theorem [6, 7, 8] which determined that a sample spacing of *circa* 2.5° would have been sufficient,

$$\Delta\theta = \frac{2\pi}{2\left(\mathrm{ceil}\left(k_0\rho_0\right) + n_1\right) + 1} \tag{11}$$

Here, n_1 is a positive integer that depends upon the accuracy required (*e.g.* n_1 = 10 [8]), k_0 is the free-space wave number, and ρ_0 is the maximum radial extent (MRE) [6, 7, 8]. In the original work [7], this irregularly spaced data was re-tabulated, using cubic spline interpolation, so that the data points were arranged on an equally spaced, monotonic grid in order that the necessary fast Fourier transform (FFT) based post processing could be utilised. Polar (*i.e.* amplitude and phase) interpolation was utilised where the re-tabulation was performed separately on the square root of the magnitude of the field and the phase function. The phase data was first unwrapped by changing all absolute jumps of greater than π to their 2π complement so as to remove any ±π phase discontinuities that would otherwise upset the interpolation process [8]. Following the interpolation, the phase was wrapped back into the modulo 2π angular range.

In order that an estimate of the upper bound error that this approximation introduces could be obtained, the regularised data was interpolated back onto the irregularly spaced measurement grid using sampling function, *i.e.* Whittaker, interpolation [8]. This sinc function interpolation scheme is rigorous, as the acquired data is spectrally band-limited however it relies upon the data being tabulated on a uniformly spaced grid. Thus; it cannot be used in place of the approximate polynomial regularisation method. Figure 2 below contains a representative plot showing the measured data which is plotted together with the reconstructed data that was formed from the regularised data set. Plotted with these traces is the 21 point "boxcar" mean average of the equivalent multipath level (EMPL) that can be taken to constitute an upper bound uncertainty level for this data regularisation process [8]. Here, the EMPL trace is more than 75 dB below the boresight values and *circa* 60 dB lower than the antenna pattern in the region of the wide-out side-lobes. This pattern data was used in [7] to verify the multipath suppression technique, *cf.* Figures 5, 6 and 7 of that paper. The processing that was demonstrated and validated in [7, 8] will be repeated

here for the sake of comparison. However, as the generalised processing technique presented above does not necessitate this sort of data regularisation the uncorrected irregularly sampled data was used as the starting point for the new post-processing algorithm.

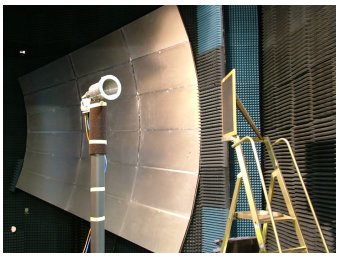

Fig. 1 X-band corrugated horn AUT installed within QMUL CATR shown together with 0.6 m by 0.6 m reflecting plate, shown to right of picture.

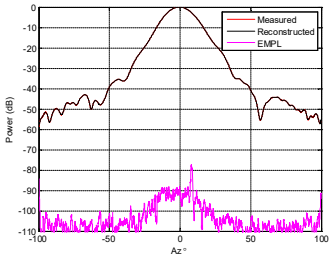

Fig. 2 Upper bound uncertainty of data regularisation process, equivalent multipath level shown in magenta and used as a measure of adjacency.

Figure 3 and Figure 4 below contain, respectively, plots of the great-circle far-field co-polar amplitude and phase patterns of the AUT. Here, the red unperturbed (reference) traces were taken without the reflecting plate, *cf.* Figure 1. Conversely, the blue traces were taken with the reflecting plate installed within the chamber and they clearly show the effects of the additional scattering as a spurious large amplitude side-lobe which is visible in the plot at around $\theta = 50°$. The magenta trace represents the conventional interpolation and FFT based mode filtering post-processing as reported in reference [7] whereas the black trace denotes the more sophisticated inverse-matrix based post-processing technique presented above in Section II.

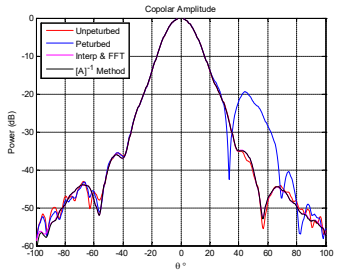

Fig. 3 Far-field amplitude plot of horn measured unperturbed and perturbed and compared against two different scattering suppression algorithms.

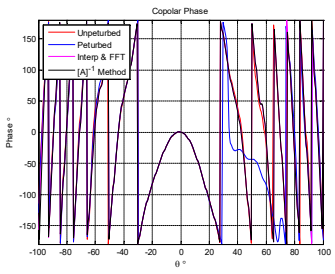

Fig. 4 Far-field phase plot of horn measured unperturbed and perturbed and compared against two different scattering suppression algorithms.

The measured far-field great circle pattern cut with scattering contamination, *i.e.* the perturbed measurement (blue-trace), was post-processed using conventional [7] (magenta-trace) and new (black-trace) generalised mode orthogonalisation and filtering algorithm, described above is presented in Figure 5. From inspection of these plots, it can be seen that the effects of the spurious scatterer have been very effectively suppressed in both the amplitude and phase plots as the unperturbed and processed perturbed traces are clearly in very encouraging agreement. This is further illustrated in Figure 5 which compares the two filtered far-field pattern cuts. The dB difference level is plotted in magenta and has an RMS level of -80dB which is a very encouraging result. Conversely, Figure 6 presents an equivalent plot to that shown in Figure 5 only here, the measured data was thinned so that only one in every ten data points were retained from the original far-field antenna pattern measurement increasing the angular sample spacing to circa 0.5°. Again, the RMS difference level was computed and it was also found to be -80 dB which is further confirmation of the stability and generality of this novel post-processing technique.

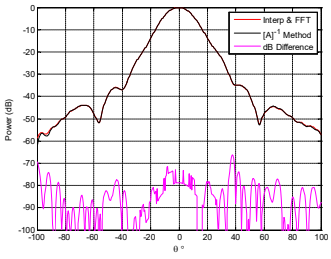

Fig. 5 Far-field amplitude plot of horn with mode filtering applied using conventional and generalised mode filtering technique.

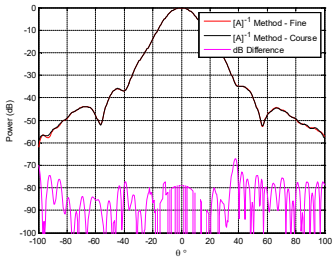

Fig. 6 Far-field amplitude plot of horn with mode filtering applied using generalised mode filtering technique with course and finely sampled far-field data.

By way of a final comparison, Figure 7 and Figure 8 respectively, present the equivalent computed CMCs plotted as a function of mode index as obtained from the standard and new generalised algorithms. Here, the CMCs are denoted by the blue trace with the band-pass filtered CMCs that are associated with the AUT being represented by the red trace. Here, it is evident that the plots are in very encouraging agreement with little difference being observed for the low order modes, which are seen at the centre of the plot. However, for the higher order modes there are some differences but these modes are not associated with the AUT and the differences will not impact upon the resulting processed far-field patterns, as presented above in Figure 5, as they will be filtered. This is very valuable as it was found that even for the case where the data had been thinned so that only one point in every 20 measured points was retained; the RMS difference level remained at *circa* -80 dB. The further thinning of the data resulted in the inability of the algorithm to compute the higher order CMCs however as those modes are not associated with the AUT their absence had no impact on the subsequent processing.

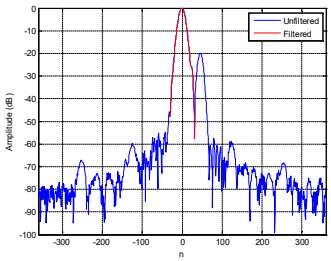

Fig. 7 Plot of amplitude of CMCs as obtained from conventional interpolation and FFT algorithm.

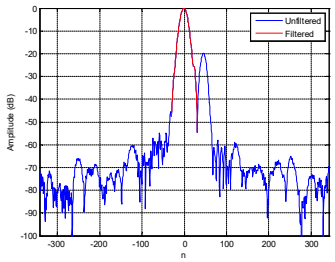

Fig. 8 Plot of amplitude of CMCs as obtained from generalised pseudo inverse matrix method.

The algorithm in effect, uses the larger number of data points to function fit a spectrum of CMCs to the measured data. The additional data points have the effect that the algorithm can more effectively suppress the effects of random noise within the measurement. The reduction in the amount of measured data merely reduces the algorithms ability to discriminate against such broadband noise sources.

Although the previous tests can be used to verify the performance of the new technique in the present intended area

of application, it was decided that it would be worthwhile if further verification could be obtained for a more demanding, limiting case. As a result, one tenth of the measured data points were taken from the finely sampled far-field cut such that the location of the points was allowed to vary randomly by up to 0.3° about the ideal angular position. Conceptually, this corresponds to a gross timing jitter within the acquisition. This is illustrated in Figure 9 which shows the original measurement, which is denoted by the red trace, with the down sampled data being represented by the black trace with crosses showing the location of the retained samples. This data was processed using the new algorithm with the resulting far-field pattern being presented in Figure 10. As before, the difference between the standard algorithm, which used all of the measured data, and the new coarsely sampled irregularly spaced data set using the new algorithm is denoted by the magenta trace. The spurious scattering has been very effectively suppressed with the RMS difference level between baseline and perturbed measurement being found to be at the -60 dB level.

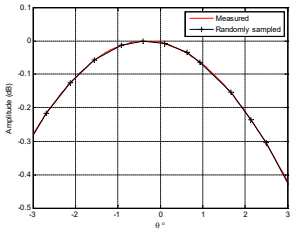

Fig. 9 Far-field main beam region showing location of points used. The irregular sample spacing is very evident.

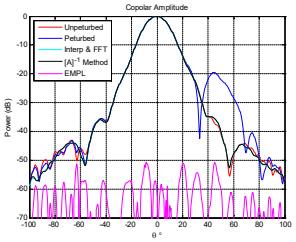

Fig. 10 Far-field amplitude plot of horn measured unperturbed and perturbed and compared against baseline result.

IV. Summary and Conclusion

For the first time, this paper describes a new, very general post processing technique that requires only a minimum amount of information about the AUT and measurement geometry, which suppresses reflections in a far-field one-dimensional frequency domain antenna pattern measurement where the data has not necessarily been acquired on an equally spaced abscissa. This technique is entirely generic in nature, can be applied to a variety of different antenna types with no specific a priori assumptions being made about the distribution of the currents over the AUT. The results presented above were produced using data that had been acquired on a regular time basis resulting in unequally spaced angular sample spacing. This is a significant advance as many far-field measurement facilities, as a result of the implementation of the positioning, control and software sub-systems, are only able to tabulate measurements on an irregularly spaced angular grid.

As has been observed previously [6, 7, 8], far-field mode orthogonalisation and filtering based scattering reduction techniques can be used with a very high degree of confidence as all of the steps within the measurement and analysis are consistent with the well-established principles of standard cylindrical near-field theory. The offset of the AUT and the resulting finer sample spacing are estimated using conventional CNF rules, and the mathematical translation of the AUT to the origin is entirely rigorous. The selection of the mode cut-off for the translated pattern is based on the physical dimensions of the AUT at its translated location. The results of the processing will reduce but clearly cannot entirely eliminate the effect of scattering [8] however, and nonetheless, a very useful improvement in measurement quality can be obtained when using this technique. As has been demonstrated, this novel frequency domain measurement and processing technique is entirely general and can be used to achieve acceptable results with use of minimal absorber or without the use of an anechoic chamber, even when testing lower gain antennas. The future work is to include obtaining further verification of the technique with the use of full-wave three-dimension computational electromagnetic simulation tools.

Acknowledgement

The authors gratefully acknowledge the funding support provided by the UK Department for Business, Energy & Industrial Strategy through the National Measurement System that enabled the work that this paper presents. The authors also extend their thanks to Mr J. Dupuy who undertook the experimental portion of this work.

References

[1] O. M. Bucci, G. D'Elia, M. D. Migliore, "A General and Effective Clutter Filtering Strategy in Near-Field Antenna Measurements," Microwaves, Antennas and Propagation, IEE Proceedings, vol. 151, no. 3, pp. 227- 235, 21 June 2004.

[2] G.E. Hindman, A.C. Newell, "Spherical Near-Field Self-Comparison Measurements", AMTA 26th Annual Meeting & Symposium, Atlanta, GA, October 2004.

[3] G.E. Hindman, A.C. Newell, "Reflection Suppression in a large spherical near-field range", AMTA 27th Annual Meeting & Symposium, Newport, RI, October. 2005.

[4] G.E. Hindman, A.C. Newell, "Reflection Suppression To Improve Anechoic Chamber Performance", AMTA Europe 2006, Munich, Germany, March 2006.

[5] D.W. Hess, "The IsoFilterTM technique: extension to transverse offsets", Post deadline Submissions, AMTA Symposium, Austin, TX, 2006.

[6] S.F. Gregson, B. Williams, G.F. Masters, A.C. Newell, G.E. Hindman, "Application of Mathematical Absorber Reflection Suppression To Direct Far-Field Antenna Range Measurements", AMTA, October, 2011.

[7] S.F. Gregson, J. Dupuy, C.G. Parini, A.C. Newell, G.E. Hindman "Application of Mathematical Absorber Reflection Suppression to Far-Field Antenna Measurements", LAPC November, 2011.

[8] C.G. Parini, S.F. Gregson, J. McCormick, D. Janse van Rensburg "Theory and Practice of Modern Antenna Range Measurements", IET Press, 2014, ISBN 978-1-84919-560-7.

[9] A.D. Olver, C.G. Parini, "Millimetre-wave Compact Antenna Test Range", JINA Nice, November 1992.G. Eason, B. Noble, and I. N. Sneddon, "On certain integrals of Lipschitz-Hankel type involving products of Bessel functions," Phil. Trans. Roy. Soc. London, vol. A247, pp. 529–551, April 1955.

[10] M.R. Hestenes, E. Stiefel, "Methods of Conjugate Gradients for Solving Linear Systems", Journal of Research of the National Bureau of Standards, Vol. 49, No.6, December 1952, pp. 409–436.

[11] C.C. Paige, M.A. Saunders, "LSQR: An Algorithm for Sparse Linear Equations and Sparse Least Squares", ACM Transactions on Mathematical Software, Vol. 8, No. 1, March 1982, pp. 43–71.